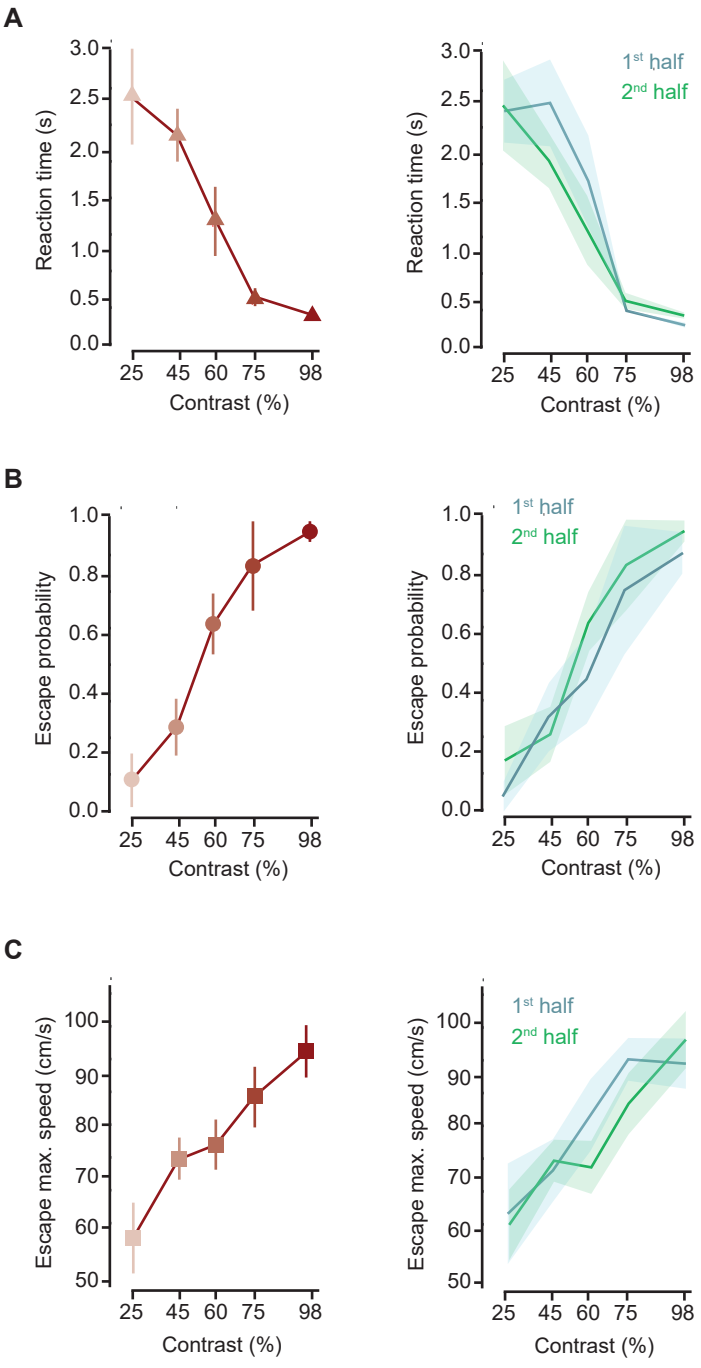

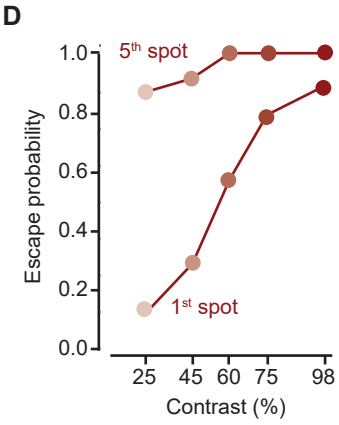

Figure S1 – Behaviour metrics computed over single mice

(A-C) Summary plots for escape behaviour metrics calculated for each mouse individually and averaged. Plots on the left were obtained with data from all trials, and in the plots on the right, trials for each contrast were split in half and the behaviour metrics calculated for each half. There is a significant dependency on contrast for all metrics (reaction time: $P=3.5\times10^{-8}$; escape probability: $P=2.1\times10^{-7}$; escape vigour: $P=1.6\times10^{-6}$, repeated measures ANOVA), and no significant difference between the metrics calculated using the first and second half of the trials ($P>0.2$ for all comparisons, two-tailed t-test comparison for each contrast), indicating that behavioural performance was stable across repeated presentations of the stimulus. Error bars and shaded areas are SEM **(D)** Escape probability after the first (as shown in Figure 1E, calculated by pooling all data) and fifth spot, during the presentation of 5 consecutive expanding spots.

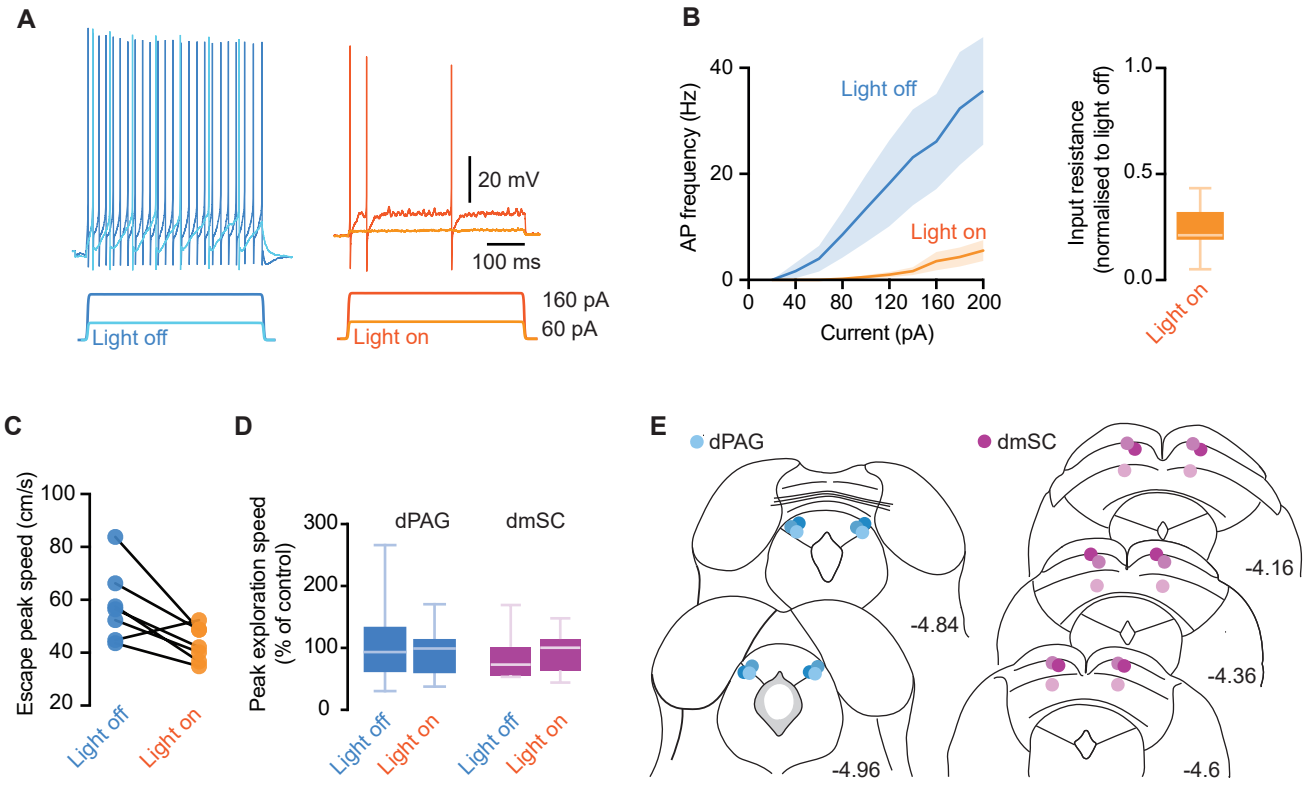

Figure S2 – iChloC activation strongly reduces neuronal firing and disrupts defensive behaviour without effects on basal locomotion

(A) Example voltage traces showing a VGluT2^{+} dmSC neuron expressing iChloC responding to current steps in control conditions (Light off) and with continuous illumination with 473nm light (Light on). **(B)** Summary relationship between current injection and action potential firing showing a very strong reduction in firing upon illumination (left, 87.9±3% reduction for all steps, P=6.09x10^{-9} t-test), as well as a strong reduction in input resistance (right, 73.2±3% reduction, P=1.23x10^{-8} t-test). Summary data are pooled from 6 dPAG and 3 dmSC cells. **(C)** For the 18% of trials in which VGluT2^{+} animals expressing iChloC in the dmSC escape from threat stimuli during continuous illumination (Light on), the vigour of escape is significantly lower when compared to escapes elicited without iChloC activation (Light off; n=7 trials, N=6 out of 9 animals, P=0.0253 paired t-test). **(D)** Movement during exploration is not affected by iChloC activation in dPAG- or dmSC-targeted animals in the absence of threat, quantified as the maximum speed in the 5s stimulation period (Light on) or control period (Light off) as a percentage of the 5s pre-stimulation period (P=0.8767 for dPAG, p=0.3443 for dmSC, U-test). **(E)** Optic fibre placements for all experiments in dPAG (N=6, blue circles) and dmSC (N=9, magenta circles), coordinates in mm and from bregma.

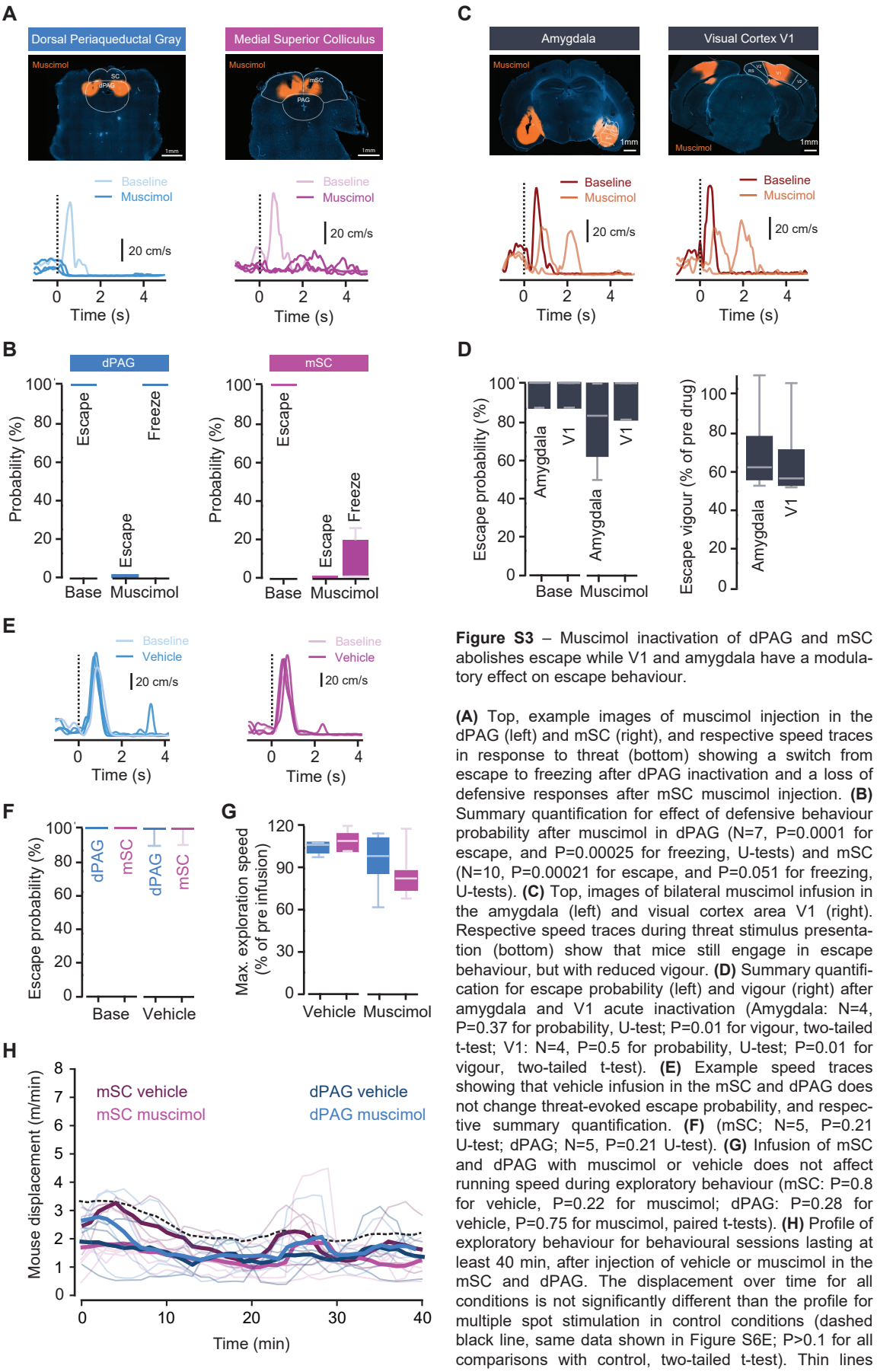

Figure S3 – Muscimol inactivation of dPAG and mSC abolishes escape while V1 and amygdala have a modulatory effect on escape behaviour.

(A) Top, example images of muscimol injection in the dPAG (left) and mSC (right), and respective speed traces in response to threat (bottom) showing a switch from escape to freezing after dPAG inactivation and a loss of defensive responses after mSC muscimol injection. **(B)** Summary quantification for effect of defensive behaviour probability after muscimol in dPAG (N=7, P=0.0001 for escape, and P=0.00025 for freezing, U-tests) and mSC (N=10, P=0.00021 for escape, and P=0.051 for freezing, U-tests). **(C)** Top, images of bilateral muscimol infusion in the amygdala (left) and visual cortex area V1 (right). Respective speed traces during threat stimulus presentation (bottom) show that mice still engage in escape behaviour, but with reduced vigour. **(D)** Summary quantification for escape probability (left) and vigour (right) after amygdala and V1 acute inactivation (Amygdala: N=4, P=0.37 for probability, U-test; P=0.01 for vigour, two-tailed t-test; V1: N=4, P=0.5 for probability, U-test; P=0.01 for vigour, two-tailed t-test). **(E)** Example speed traces showing that vehicle infusion in the mSC and dPAG does not change threat-evoked escape probability, and respective summary quantification. **(F)** (mSC; N=5, P=0.21 U-test; dPAG; N=5, P=0.21 U-test). **(G)** Infusion of mSC and dPAG with muscimol or vehicle does not affect running speed during exploratory behaviour (mSC: P=0.8 for vehicle, P=0.22 for muscimol; dPAG: P=0.28 for vehicle, P=0.75 for muscimol, paired t-tests). **(H)** Profile of exploratory behaviour for behavioural sessions lasting at least 40 min, after injection of vehicle or muscimol in the mSC and dPAG. The displacement over time for all conditions is not significantly different than the profile for multiple spot stimulation in control conditions (dashed black line, same data shown in Figure S6E; P>0.1 for all comparisons with control, two-tailed t-test). Thin lines show individual mice and thick lines show the dataset mean.

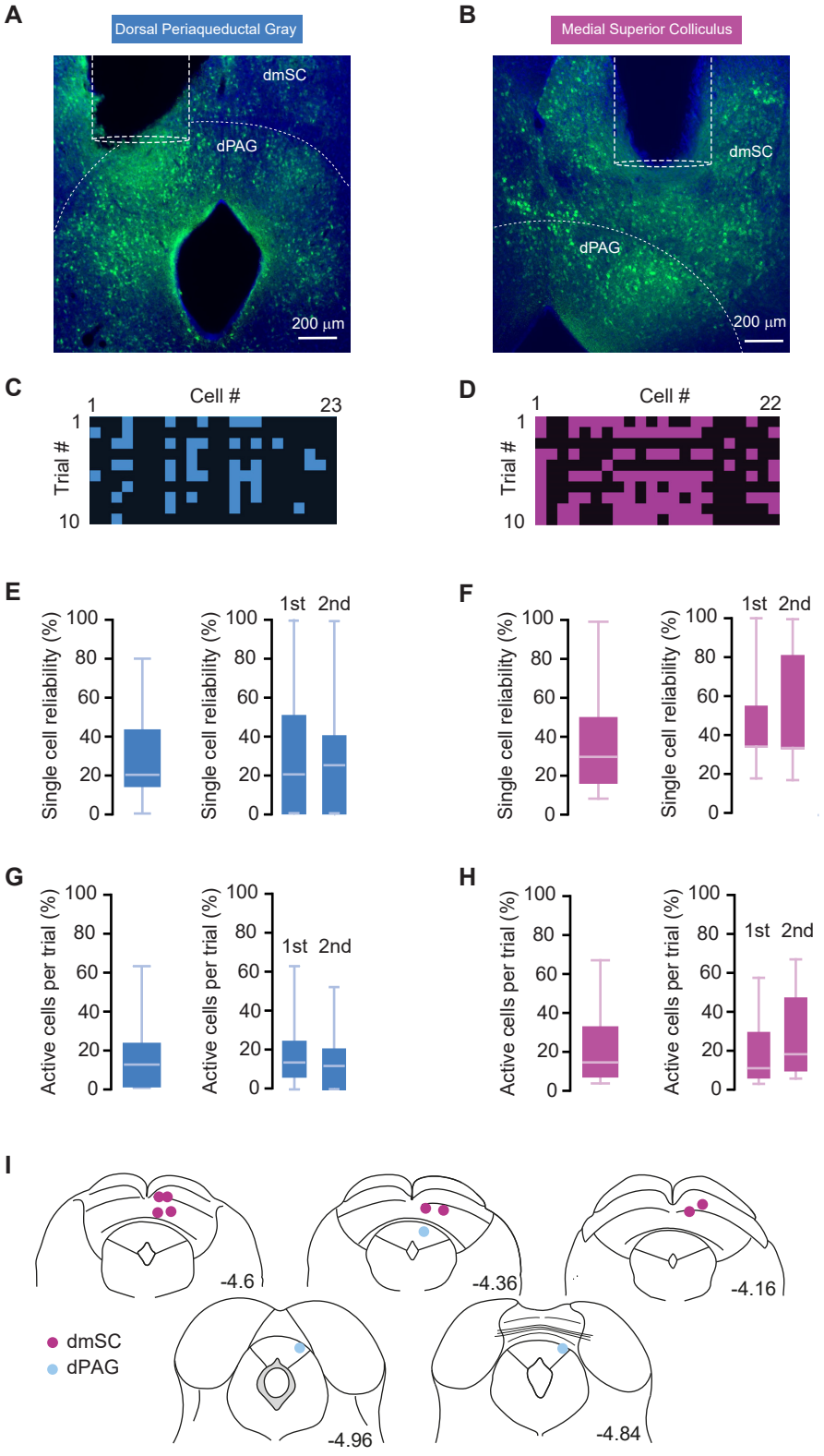

Figure S4 – The reliability and fraction of active cells is stable over multiple trials of calcium imaging

(A,B) Example images of GCaMP6s expression in VGluT2^{+} cells (green), with schematic showing GRIN lens placement in the dPAG and dmSC. **(C,D)** Raster plots showing active (colour squares) and non-active cells (black squares) in a single field-of-view (FOV) imaged over multiple trials. We imaged a total of 8 FOVs in the dPAG with a mean of 18 cells per FOV (range = [7,30]), and 11 trials per FOV; and 11 FOVs in dmSC with a mean of 20 cells per FOV (range = 7,31] and 20 trials per FOV). There was a mean of 7 escape-responding cells per dPAG FOV and 16 escape-responding cells per dmSC FOV. **(E,F)** Reliability of escape-responding cells showing a response over multiple trials for all trials (left) and for the first and second half of trials separately (right). Mean reliability across all trials was 28±3% for dPAG and 35±3% for dmSC, and stable over multiple trials (P=0.44 for dPAG, P=0.11 for dmSC, comparison between the two groups of trials, U-test). **(G,H)** Fraction of all cells in a FOV that are active on each trial for all trials and for the first and second half of trials separately (right). The active fraction across all trials was 14±3% for dPAG and 23±6% for dmSC, and stable over multiple trials (P=0.21 for dPAG, P=0.08 for dmSC, comparison between the two groups of trials, U-test). **(I)** Placement of GRIN lenses in the dmSC (magenta) and dPAG (blue circles), coordinates in mm and from bregma.

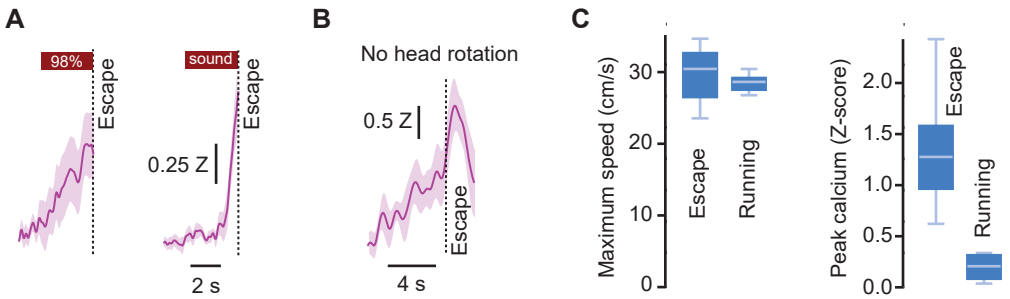

Figure S5 – Calcium activity in the dmSC does not reflect head rotation and rises with different slopes, while dPAG activity increases specifically during escape and not running.

(A) Average population activity in the dmSC for escape trials in reponse to 98% contrast spots and sound stimuli. The slope of the signal rise is steeper for sound-evoked escape. **(B)** Average calcium signal for population activity in the dmSC during escape trials where the mouse was already facing the shelter and did not rotate the head (N=5 trials). **(C)** Summary quantification of dPAG population activity calcium signals during threat-evoked escape and spontaneous foraging running bouts of similar speed (N=6 running bouts and N=6 escape trials, speed not significantly different, P=0.64, t-test), showing that activity increase in the dPAG is specific for escape (P=0.0018, t-test).

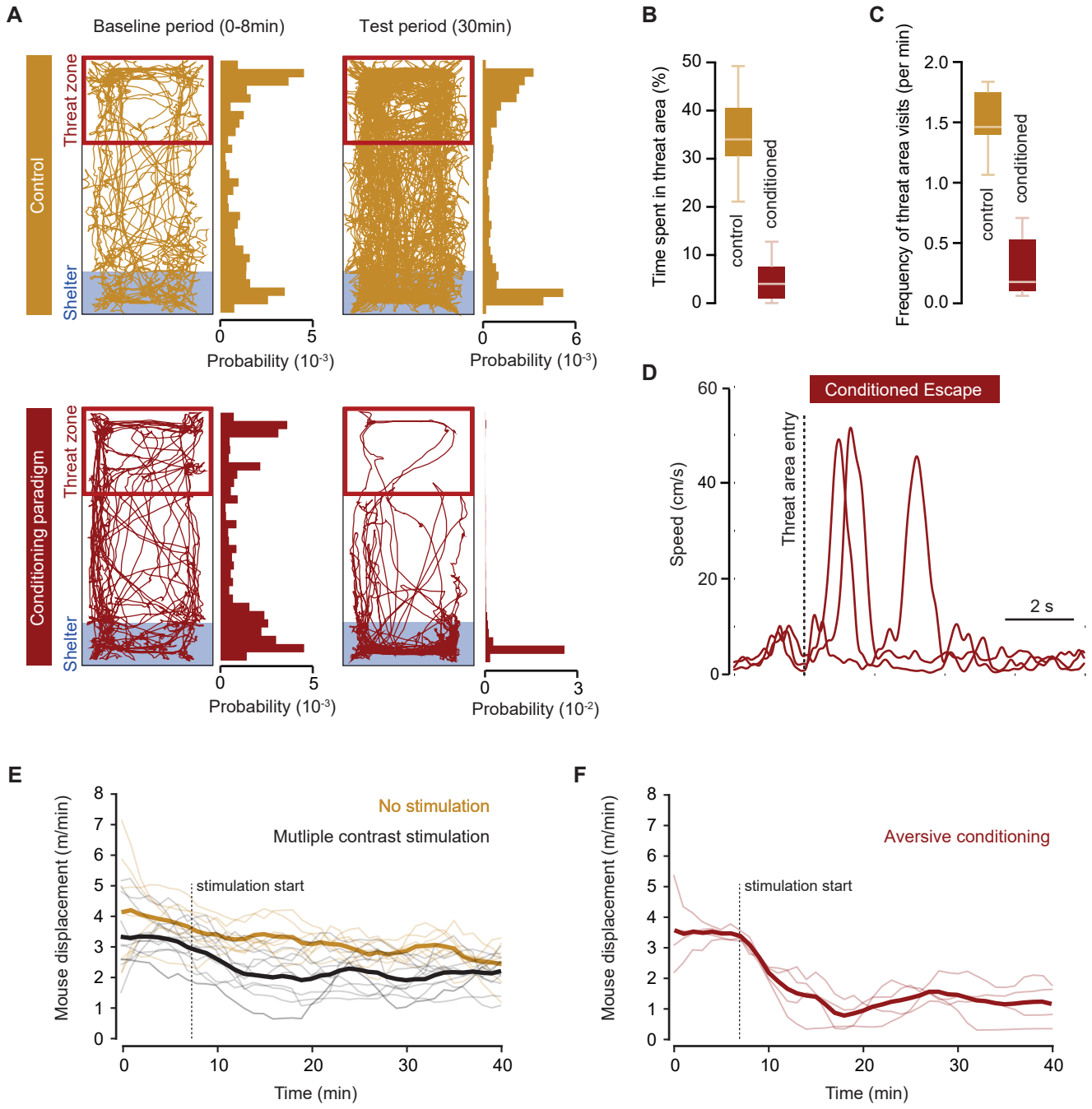

Figure S6 – Repeated high-contrast visual stimulation causes place aversion, reduction in exploration and spontaneous escape

(A) Traces and probability distributions for the location of two example animals during free exploration (top), and before and after a high contrast visual stimulation conditioning paradigm (bottom), showing avoidance of the threat area after conditioning (bottom right). **(B)** Time spent in the threat area decreases with aversive conditioning (35.1±3.5% for naïve animals vs 5.1±2.0% after conditioning, N=7 mice, $P=2.2x10^{-5}$, two-tailed t-test). **(C)** The frequency of visits to the threat area by the animals also decreases significantly after conditioning (1.51±0.10 visits/min for naïve animals vs 0.30±0.12 after conditioning, N=7 mice, $P=1x10^{-4}$, two-tailed t-test). **(D)** Example speed traces from three animals showing spontaneous escape after conditioning. **(E)** Profile of exploratory behaviour during behavioural sessions of multiple contrast stimulation (black, data taken from the animals that generated the dataset for Figure 1) and no stimulation for comparison (orange). Exploration decays over time and the decay is accelerated by visual stimuation, but the two curves are not significantly different over time (2.4±0.3 m/min at 40 min for control vs 2.0±0.3 with visual stimulation, P=0.16, two-tailed t-test). **(F)** Same quantification as in E for sessions of aversive conditioning. Aversive conditioning significantly reduces exploratory behaviour (1.2±0.3 m/min after conditioning, P=0.018 against no stimulation and P=0.039 against multiple contrast stimulation, two-tailed t-test). Thin lines show individual mice monitored for 40 min and thick lines show the dataset mean.

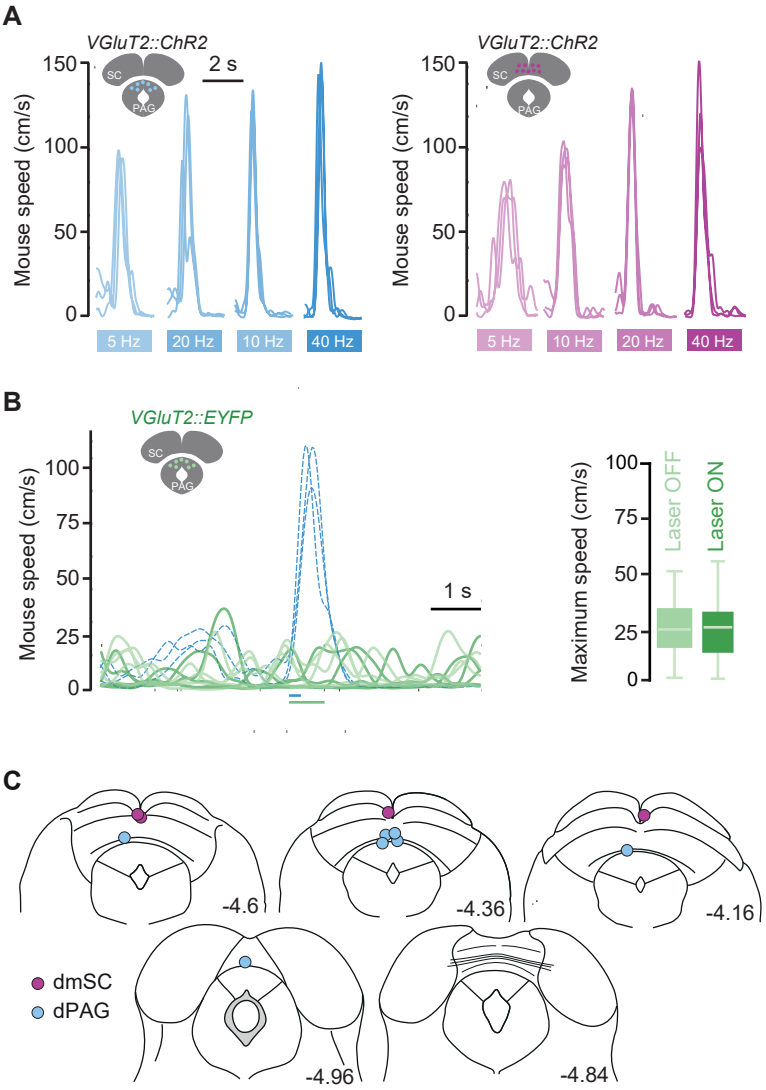

Figure S7 – ChR2 activation causes escape at different stimulation frequencies while stimulation of EYFP-expressing cells does not modify behaviour.

(A) Example speed traces for dPAG (left) and mSC (right) ChR2 stimulation at different frequencies (10 pulses) and high light intensities, showing robust escape behaviour for 5 to 40Hz stimulation. **(B)** Left, speed traces for 473nm light stimulation (40Hz, 30 pulses) of one mouse expressing EYFP in the dPAG (dark green), showing no change in running speed. Light green traces show similar speed profiles for the same mouse entering the stimulation area with stimulation off. Blue dashed traces are from a different animal expressing ChR2 in the dPAG (40Hz, 10 pulses), for comparison. Right, summary data for EYFP control stimulation in dPAG (running speed not significantly different between laser on and off, P=0.48, U-test, N=236 trials from 3 animals). **(C)** Optic fibre placements for ChR2 stimulation in the dmSC (magenta) and dPAG (blue circles), coordinates in mm and from bregma.

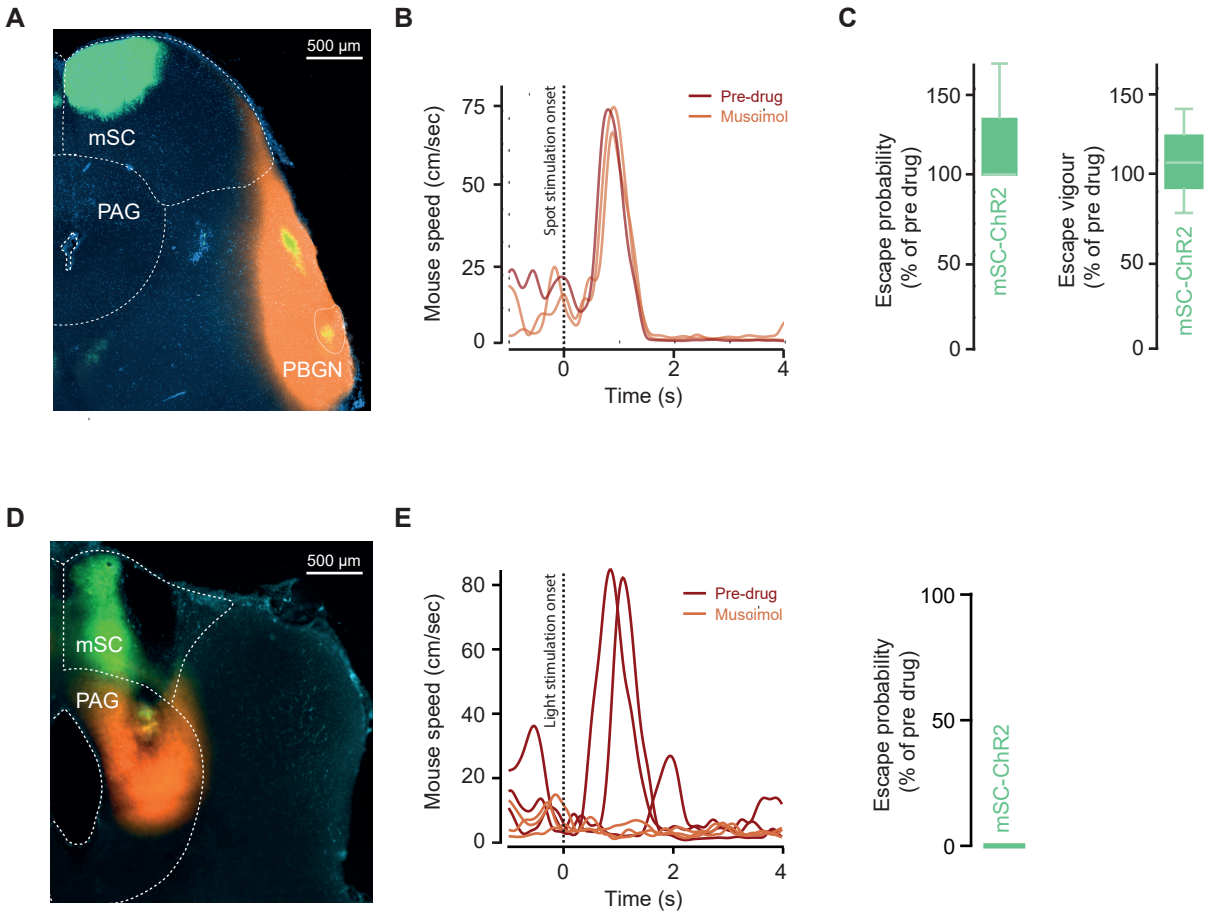

Figure S8 – Escape evoked by mSC-VGluT2::ChR2 or a visual threat is unaffected by acute PBGN inactivation, while inactivation of the PAG abolishes it.

(A) Image showing expression of ChR2-EYFP in the mSC (green) with projections to the PBGN (yellow) and muscimol infusion (orange). **(B)** Speed traces for spot-evoked escape reponses from one mouse before and after acute PBGN inactivation. **(C)** Summary data for escape probability and vigour during mSC optogenetic stimulation and PBGN acute inactivation, showing no difference (N=3 animals, P=0.80 for probability; P=0.70 for vigour, U-test). **(D)** Image showing expression of ChR2-EYFP in the mSC (green) and muscimol infusion in the PAG (orange). **(E)** Speed traces (left) and summary data (right) showing that mSC optogenetic-evoked escape is abolished by PAG acute inactivation (N=3 animals, P=0.0297 for probability, U-test).

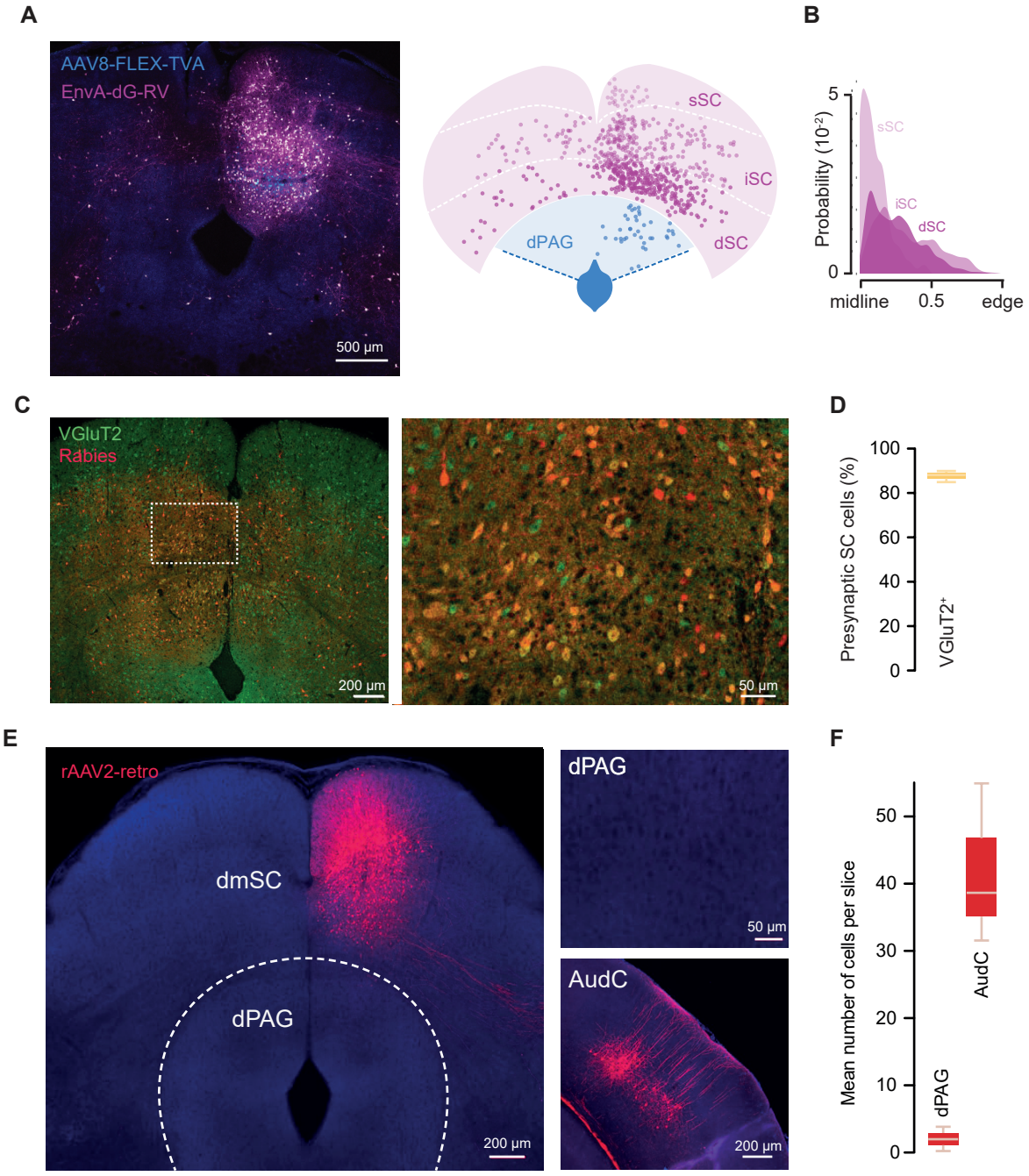

Figure S9 – dPAG neurons receive input from mainly excitatory cells in the SC and do not project back to the SC.

(A) Image showing starter dPAG VGluT2$^+$ cells expressing both TVA-GFP and RV-mCherry and presynaptic cells expressing RV-mCherry only (left), and corresponding schematic (right) illustrating the position of starter dPAG (blue) and presynaptic SC cells (pink) across deep, intermediate and superficial SC layers (same as shown in Figure 4A). **(B)** Kernel density estimation curves for the axial position of presynaptic SC cells for each layer. **(C)** Image showing presynaptic cells in the mSC infected with rabies virus (red) from starter neurons in the dPAG of a VGlut2::EYFP mouse (left). Box indicates area magnified shown on the right. Yellow cells are excitatory mSC presynaptic neurons. **(D)** Summary quantification of the fraction of presynaptic cells in the mSC that express VGluT2$^+$. **(E)** Image showing injection of rAAV2-retro in the mSC (left) and no retrogradely labelled cells in the dPAG (right, top). Right, bottom: retrograde labelling in the auditory cortex for comparison. **(F)** Summary quantification for retrogradely labelled cells after mSC rAAV2-retro infection in the dPAG and auditory cortex. In all plots error bars are SEM.

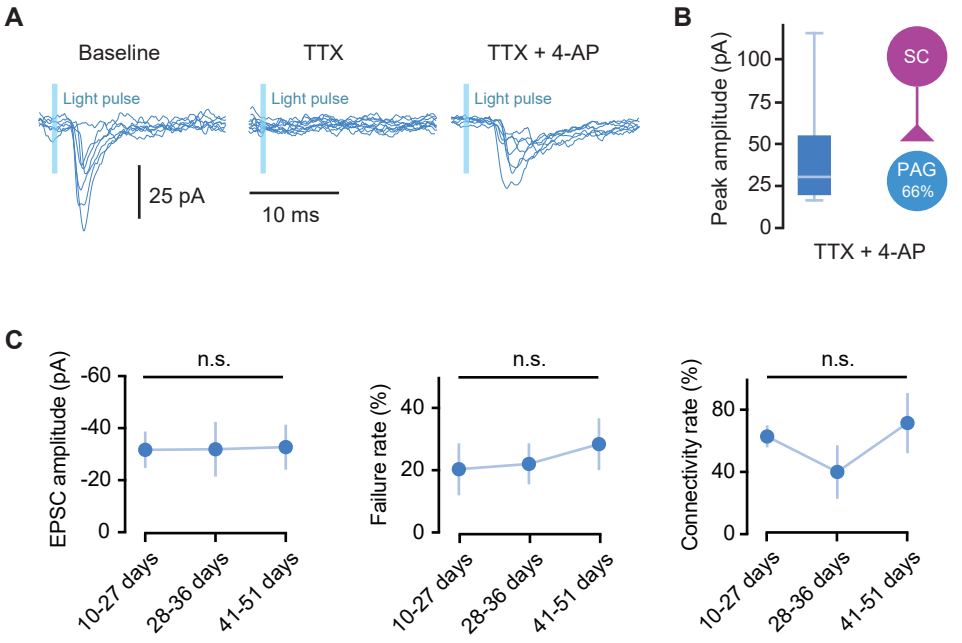

Figure S10 – dmSC-dPAG excitatory connections are monosynaptic and properties do not change with long transfection times

(A) Example current traces for one dPAG VGluT2^{+} cell showing optogenetically-evoked EPSCs from the dmSC (left) that are blocked by TTX (middle) and recovered by 4-AP (right), and thus confirming the presence of a monosynaptic connection. **(B)** Summary data for peak dmSC-dPAG EPSC amplitudes and connectivity rate in the presence of TTX and 4-AP. **(C)** Summary data showing that the properties of the dmSC-dPAG connection do not change with number of days after viral transfection of ChR2, and remain weak and unreliable (P=0.78, 0.51 and 0.33 for amplitude, failure rate and connectivity rate, respectively, Kruskal-Wallis test; N=15)

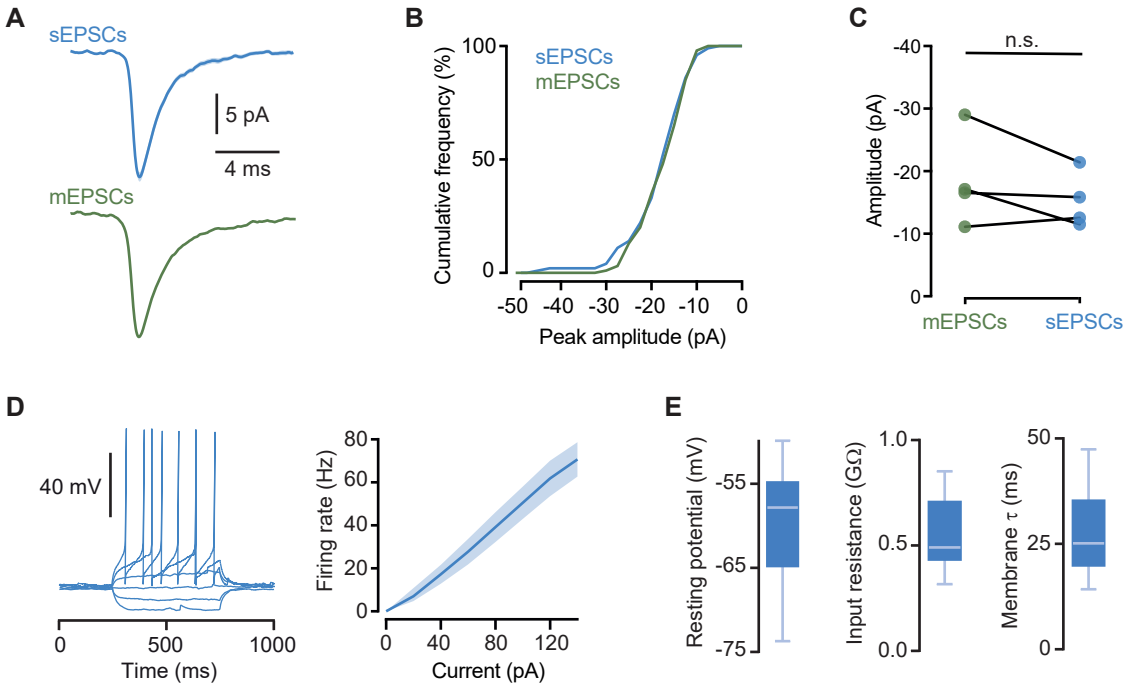

Figure S11 – Synaptic and biophysical properties of excitatory dPAG neurons

(A) Average waveforms for sEPSCs and mESPCs (recorded in TTX) in one cell, and respective cumulative histogram for peak amplitudes **(B)**. **(C)** Peak amplitude of sEPSCs and mEPSCs in not significantly different (n=4 cells, P=0.18, 0.79, 0.9 and 0.36 respectively, Kolmogorov-Smirnov test for 100 events in each condition per cell). **(D)** Example trace of current step injections in a VGluT2$^+$ dPAG neuron (left) and summary current-frequency relationship (right, shaded area is SEM). **(E)** Summary quantification of resting membrane potential, input resistance and membrane time constant for VGluT2$^+$ dPAG neurons.

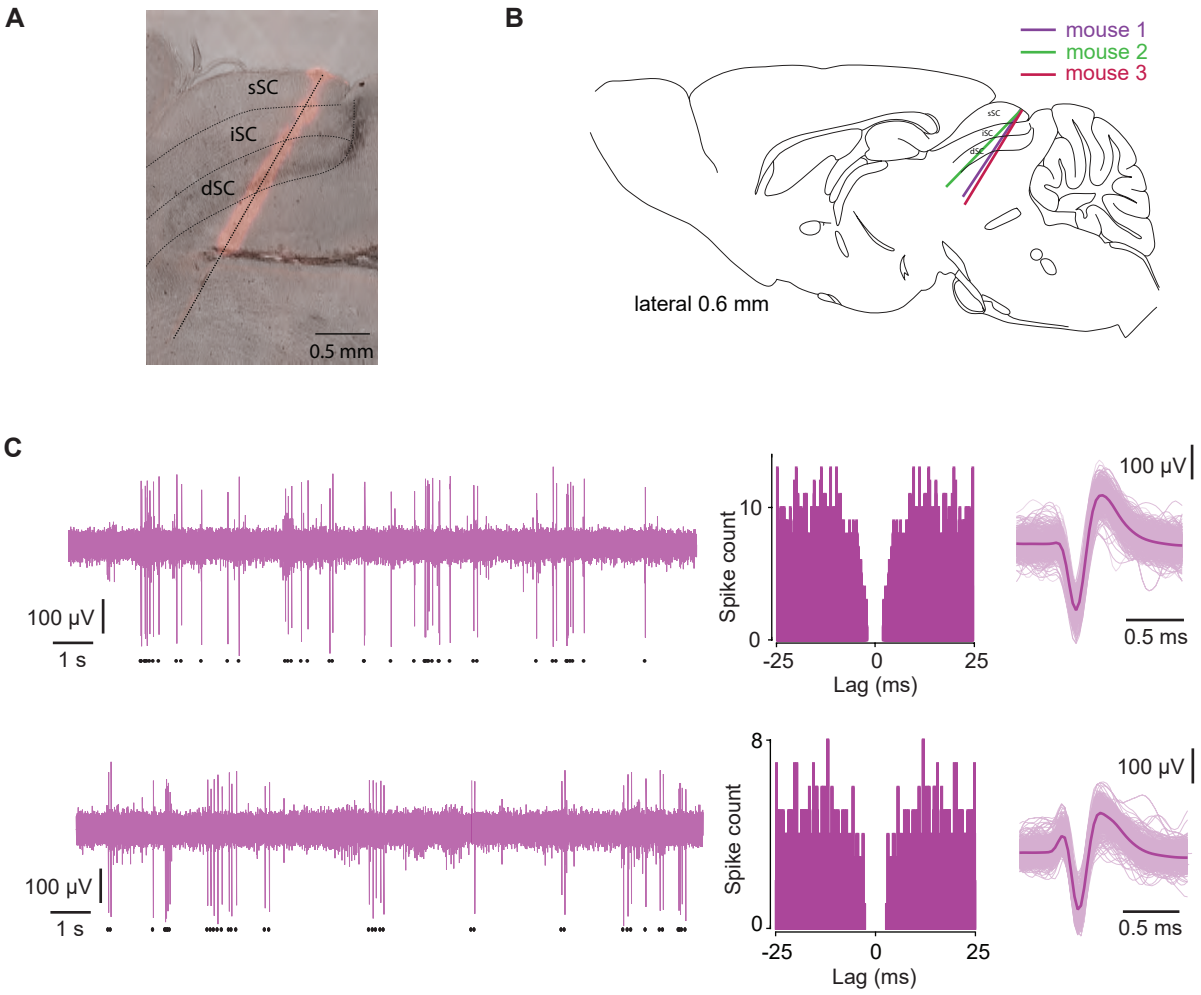

Figure S12 – Silicon probe anatomical placement and examples of dmSC single units

(A) Example image showing the track left by one probe stained with DiI, superimposed on a bright-field image of a 30um sagittal slice. **(B)** Schematic illustrating the probe track in each of the three animals used (sagittal section, 0.6mm lateral to the midline, taken from Paxinos & Franklin). **(C)** Two examples of dmSC single units (top and bottom). Left, raw voltage trace from the channel with the strongest signal for the unit of interest (black symbols below indicate all spikes detected for the unit). Middle, auto-correlogram of spike times calculated in bins of 1/30ms. Right, superimposed action potential waveforms chosen randomly from the whole recording (light colour) and average waveform (dark colour).

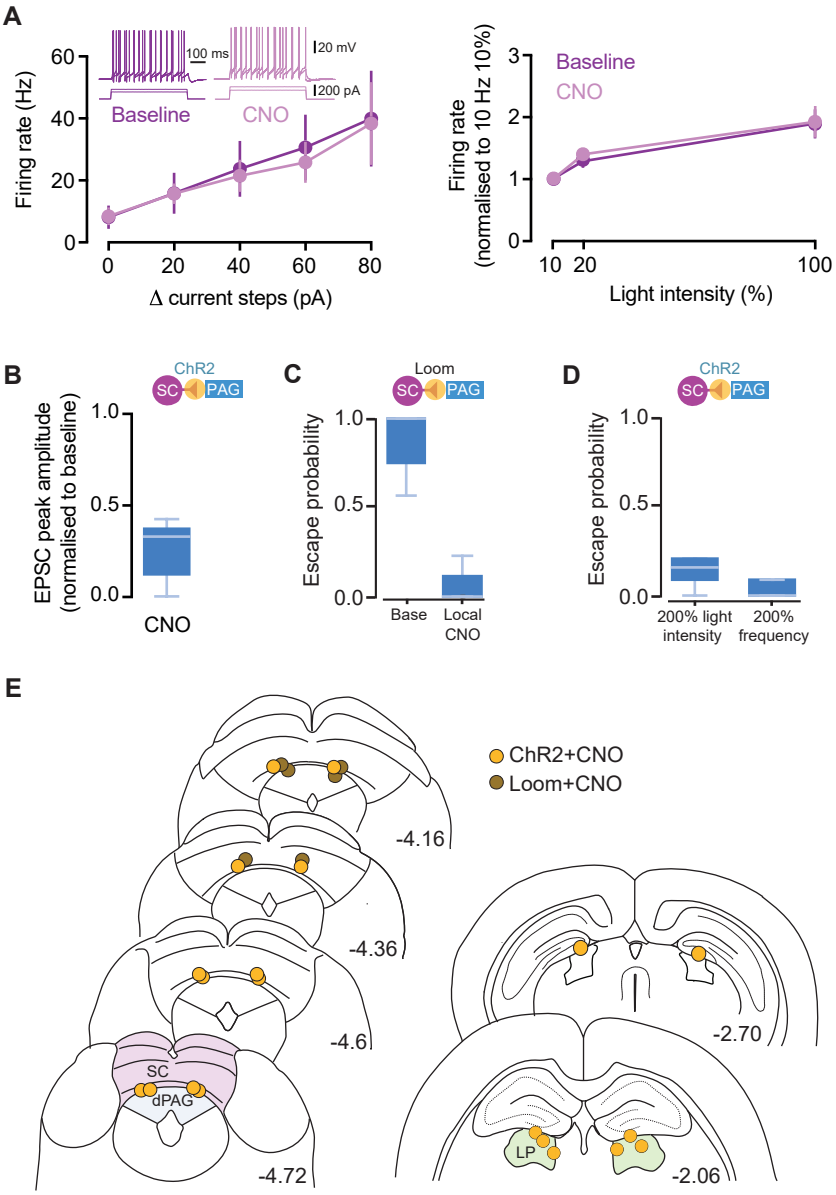

Figure S13 Controls and cannulae placements for chemogenetic inactivation experiments

(A) Summary *in vitro* data for hM4D-neurexin:ChR2 VGluT2^{+} dmSC neurons before (baseline) and after CNO application (CNO), showing no effect of CNO on action potential firing in response to current injection (left, N=6 cells, P=0.1875 Wilcoxon test; inset shows example traces to two current steps) or to 473nm light-evoked ChR2 activation (right, N=9 cells, P=0.25 Wilcoxon test). **(B)** CNO application reduces dmSC-dPAG excitatory synaptic transmission by 71±7% (N=10 cells, P=6.19x10^{-6} two-tailed t-test between baseline and CNO). **(C)** Disrupting mSC-dPAG synapses with CNO microinfusion blocks visually-evoked escape behaviour (N=3 mice, P=0.036 U-test). **(D)** Doubling the intensity or frequency of mSC stimulation while locally blocking mSC-dPAG synapses is not sufficient to rescue escape behaviour (N=5 mice, P=0.11 for intensity, U-test; P=0.42 for frequency, U-test; both comparisons against escape probability after local block in baseline conditions shown in Fig.4L). **(D)** Cannula placements for local inactivation experiments with CNO at the SC-PAG synapse (left panel) and at the SC-LP synapse (right panel). The tip of the internal cannulae is indicated by yellow circles (for experiments with optogenetic stimulation of dmSC VGluT2^{+} cells) and brown circles (for experiments with visual stimulation). Coordinates are in mm and from bregma.

Target region	Coordinates (mm)			Cannula (mm)		Volume (µL)
	ML	AP	DV	Dual	Internal	
Amygdala	±2.80	−1.60b	−4.75	—	−0.75	1.2-1.5
Periaqueductal gray, dorsal[1]	±0.60	−0.45λ	−2.20	1.2	−0.50	0.6-0.8
Superior colliculus, medial	±0.50-0.60	−0.20λ	−1.50	1.0-1.2	−0.50	1.0
V1	±2.50	+0.50λ	−0.30	—	−0.75	1.0
Parabigeminal nucleus[2]	±2.40	−0.35λ	−2.75	—	−0.75	0.8

[1] For combined optogenetic experiments in Fig S8, mSC VGluT2::ChR2 and optic fiber implant performed in same surgery

[2] Performed in mSC VGluT2::ChR2 animals with optic fiber implanted in same surgery. Infusion cannulae angled 15º lateral from zenith.

Table S1 – Experimental parameters for pharmacological inactivation of circuit elements.

Cannula implant coordinates are specified from bregma (b) or lambda (λ). The final target depth is the sum of the DV and Internal lengths. When dual implants were used, the width between the cannulae is given.